ECS Transactions, 58 (2) 183-190 (2013)
10.1149/05802.0183ecst ©The Electrochemical Society

Validation of $Nd_2NiO_{4+\delta}$ as Oxygen Electrode Material for Intermediate Temperature Solid Oxide Cells with LSGM Electrolyte

A. Montenegro-Hernández, L. Mogni, A. Caneiro

CNEA-CONICET. Departamento de Caracterización-Materiales, Centro Atómico Bariloche, Av. Bustillo 9500. S.C. de Bariloche, CP 8400, Rio Negro Argentina

The oxygen reduction reaction (ORR) was studied by Electrochemical Impedance Spectroscopy (EIS) for $Nd_2NiO_{4+\delta}$ (NNO) electrodes deposited on $La_{0.9}Sr_{0.1}Ga_{0.8}Mg_{0.2}O_{2.85}$ (LSGM) electrolyte. The influence of NNO microstructure on the electrochemical performance was evaluated. The EIS measurements were carried out as a function of temperature ($500<T<750^oC$) and oxygen partial pressure ($10^{-4}<pO_2<1atm$). Three contributions associated with the ORR were identified: at high (HF), medium (MF) and low frequencies (LF). The HF contribution was associated with oxygen ion transfer trough electrode/electrolyte interphase. The MF contribution was attributed to oxygen ions diffusion within the NNO. The LF contribution was related to O_2-dissociative adsorption for NNO obtained by chemical routes, where the particle sizes are smaller. If NNO were obtained by Solid State Reaction, the LF element was associated with a convolution of dissociative adsorption and gas diffusion processes.

Introduction

The search of new electrode materials applied to Fuel Cell technology is an active field of research (1). Particularly, oxygen electrode materials for Solid Oxide Cells (SOC) must fulfill several requirements such as high electrocatalytic activity for oxygen redox reaction, and good thermal and chemical compatibility with solid electrolytes (2–4).

The $Ln_2NiO_{4+\delta}$ (Ln = lanthanide) compounds belong to the Ruddlesden-Popper series and can incorporate oxygen ions into interstitial sites in the LnOx layer. These O-ions present high mobility giving place to high ionic conductivity by interstitial oxygen diffusion (5). Therefore, these nickelates could be oxidized under anodic polarization, producing Ni^{+3} ions and oxygen interstitials defects, which increase the electrocatalytic properties and make these compounds suitable to be operated in electrolyzer mode (6). The $Ln_2NiO_{4+\delta}$ also presents Thermal Expansion Coefficients (TEC) similar to those of widely used Solid Oxide Fuel Cell (SOFC) electrolytes: $Zr_{0.92}Y_{0.08}O_{1.96}$ (YSZ), $Ce_{0.9}Gd_{0.1}O_{1.96}$ (CGO) and $La_{0.9}Sr_{0.1}Ga_{0.8}Mg_{0.2}O_{2.85}$ (LSGM) (7–9). However, one drawback of these materials is the chemical reactivity with CGO and YSZ electrolytes at operation (600 to 800 ºC) or adhesion temperatures (900 - 1000 ºC) (10–15). Recently, we have reported chemical reactivity between $Nd_2NiO_{4+\delta}$ (NNO) and YSZ or CGO electrolytes during accelerated aging tests above 1000 °C for 2 h and 72 h, respectively

(12). This fact suggests that these electrode/electrolyte compounds would be unsuitable for operating during long periods of time.

NNO has been recently reported as potential oxygen electrode for both SOC applications: Fuel and Electrolizer (SOFC and SOEC); due to its reversibility on the O_2-redox reaction (5,6,16,17). Some authors found that cells with NNO electrodes display current densities 3 or 4 times higher than similar cells tested with conventional $La_{0.8}Sr_{0.2}MnO_3$ (LSM) oxygen electrodes (5). This result was associated to the presence of interstitial oxygen which promotes both ionic and electronic conductivities (5,6,16,17).

In this work, we present a study of the electrode mechanism by using Electrochemical Impedance Spectroscopy (EIS) on NNO/LSGM/NNO symmetrical cells between 500 and 750 °C and oxygen partial pressure pO_2 between 10^{-4} and 0.2 atm. No decomposition or chemical reaction between LSGM and NNO was found. The influence of the electrode microstructure was analyzed using NNO prepared by three different synthesis methods: the conventional Solid State Reaction (SSR) and two chemical routes (hexamethylenetetramine (HMTA) and citrates (CIT)). We include previous results obtained using NNO/CGO/NNO cells (12) in order to discuss the effect of reactivity on electrode/electrolyte response.

Experimental

Samples Preparation

NNO powders were synthesized by three different methods. The first one, HMTA method (18) uses Nd_2O_3 and $Ni(CH_3COO)_2{\cdot}H_2O$, with analytic grade as precursors. Stoichiometric amounts of precursors were dissolved in acetic acid with hexamethylenetetramine (HMTA) and acetylacetone, in a (ligand: metal) 3:1 molar ratio. The solution was refluxed and heated until a brown gel was obtained. This gel was fired at 400 °C and finally annealed at 950 °C. The obtained sample was named NNO-HMTA.

The second one was the citrates method, which uses Nd_2O_3 and metallic Ni as raw materials. In this case, the precursors were dissolved in diluted nitric acid and dried at 80 ºC. Citric acid and ethylene glycol dissolved in distilled water were added to the dry nitrates and the mixture was stirred until a transparent solution was obtained. The liquid was slowly evaporated until a polymer was formed. The polymer was fired at 400 ºC to eliminate organic products and the remaining powders were heat treated at 950 ºC. This sample was named NNO-CIT.

The third preparation method was the standard SSR method. Nd_2O_3 and NiO were mixed in stoichiometric ratio, ball milled and finally heated at 1200 ºC. This sample was named NNO-SSR. As noted above, both chemical routes decrease the synthesis temperature from 1200 to 950 °C.

Symmetrical NNO/LSGM/NNO cells were conformed depositing a porous layer of electrode material on both sides of a dense LSGM electrolyte. The dense electrolyte was obtained pressing fine powder of LSGM (Fuel cells materials) and sintering at 1500 ºC for 4 h. NNO slurries were prepared mixing NNO powders (NNO-HMTA, NNO-CIT and

NNO-SSR) with polyvinyl butyral (2% w/w), polyetileneglycol (1% w/w), ethanol (30% w/w) and α- terpineol (27% w/w). The LSGM substrates were covered with the NNO ink onto both flat sides by spin coating. Afterwards, the symmetrical assemblies were heat treated at 1000 ºC for 1 h to promote electrode/electrolyte adhesion.

Samples Characterization

The samples were characterized by X-ray diffraction (XRD) for phase identification and phase purity assessment. The compatibility between NNO and LSGM electrolytes was checked by XRD in a similar way than that used to study the chemical reactivity between NNO and CGO electrolyte (19). NNO-HMTA electrode material and electrolyte powders were mixed in a 1:1 weight ratio annealed at 900, 1000 and 1050 ºC for 72 h.

The microstructures of top surfaces of the electrodes and NNO/CGO cross-sections were examined by Scanning Electronic Microscopy (SEM). The electrochemical characterization of porous NNO electrodes was carried out through EIS measurement. The effect of microstructure on the electrode reaction mechanism was evaluated on symmetrical cells within the range of 500 to 750 °C. These EIS measurements were carried out by using a frequency response analyzer (FRA) coupled to an AUTOLAB potentiostat. EIS spectra were collected varying pO_2 within the range of 10^{-4} to 1 atm. Controlled pO_2 atmospheres were provided by an electrochemical system composed of an oxygen pump and an oxygen sensor and Ar as gas carrier (20). The resulting spectra were fitted with electrical equivalent circuits using Zview program (21). These results were used to study the oxygen electrode mechanism reaction. Before and after the EIS measurements cathode surfaces were characterized by XRD. In both cases the presence of secondary phases or NNO decomposition were not detected.

Results and Discussion

Characterization of the Electrode Microstructure and Chemical Compatibility with Electrolyte

The SEM study shown that different NNO microstructures can be obtained by using the three different synthesis methods (19). The HMTA sample presents submicron agglomerates constituted by small grains with low connectivity. The microstructure of CIT sample is very different to that of HMTA, displaying agglomerates with irregular shaped and dense surfaces. The SSR method produces agglomerate powders formed by grain with sizes larger than 1μm (19).

Chemical reactivity between NNO-HMTA and LSGM powder mixture was not detected trough XRD in powder after being heated at 1000 °C for 72 h. The XRD patterns (results not shown here) only present the diffraction peaks of the starting materials (NNO and LSGM). Nevertheless, two reflections identified as Nd_2O_3, were observed in the powder mixture after being treated 72 h at 1050 °C.

Effect of Microstructure on the Electrochemical Performance of NNO

The limiting steps of the Oxygen Reduction Reaction (ORR) were determined trough EIS after proving that the NNO electrode and the LSGM electrolyte did not react at 1000 °C. The influence of the electrode microstructures on the reaction mechanism was analyzed by using NNO obtained by the three different synthesis methods.

Figure 1 shows a cross section SEM image of NNO-HMTA, NNO-CIT and NNO-SSR electrodes on LSGM substrates after the EIS measurements. The NNO-CIT grains appear to be more connected than those of the NNO-HMTA electrode. The NNO-SSR electrode presents agglomerated particles with larger particle size compared to those electrodes obtained by both soft chemical routes. No cracks were observed for the three cathodes studied. This fact is expected, since LSGM and NNO materials display similar TEC (6). The cross sections show a film thickness of approximately 15 μm for the three electrodes.

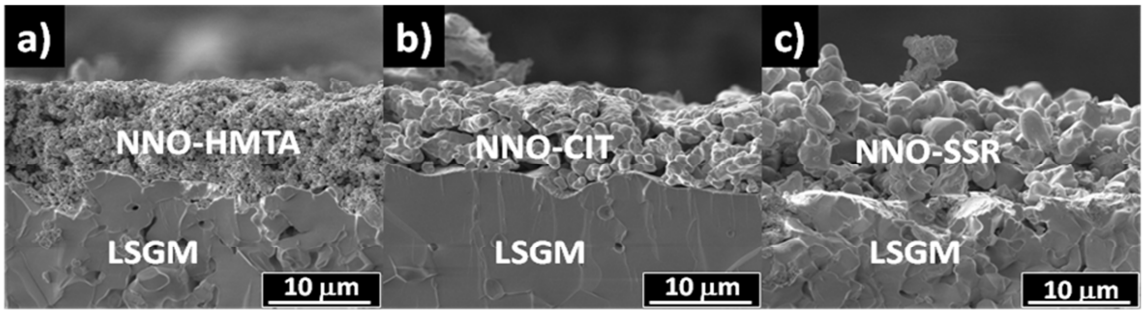

Figure 1. SEM images of cross sections of electrode/electrolyte interphase for (a) NNO-HMTA, (b) NNO-CIT and (c) NNO-SSR electrodes on LSGM substrate after EIS measurements.

The Arrhenius plots of the total Area Specific Resistance (ASR) of the three cells studied are shown in Figure 2 a). All of them show a thermally activated behavior within the whole temperature range. The activation energy values are 1.15, 1.30 and 1.35 for NNO-HMTA, NNO-CIT and NNO-SSR, respectively. In contrast to those previously found for NNO/CGO/NNO cells (19), the ASR values for the NNO/LSGM/NNO cells increase from NNO-HMTA to NNO-CIT and NNO-SSR. The ASR is defined as ASR= Rp*A/2 where Rp is the polarization resistance and A is the cathode geometric area. The ASR values for the NNO/LSGM/NNO cells show a uniform variation with temperature, without any break in the ASR vs Temperature slope.

It is worth to mention that the NNO-HMTA cathode deposited on LSGM electrolyte displays lower ASR values (see Figure 2 a)) than other NNO microstructures. This result is different to those previously obtained using CGO as electrolyte, where the best performance was achieved for the NNO-CIT cathode (19). The difference between NNO/CGO and NNO/LSGM behaviors may be due to the presence of reactivity between CGO and NNO (19). We have proposed that the fine microstructure of NNO-HMTA improves the kinetics of chemical reaction between NNO-HMTA and CGO. Therefore, the NNO-HMTA/CGO response is strongly affected respect to NNO-CIT/CGO and NNO-SSR/CGO cases. In other words, when LSGM is used instead of CGO as electrolyte, the ASR decreases as the particle size decreases exposing to air more active sites for ORR. In the case of the

NNO/CGO/NNO cells, a competitive effect between ORR and chemical reactivity with electrolyte affects the electrode response. Figure 2 b) shows a comparison between ASR for NNO-HMTA/LSGM/NNO-HMTA, NNO-CIT/CGO/NNO-CIT and NNO-HMTA/CGO/NNO-HMTA cells. It can be seen that, using LSGM, the ASR values obtained are much lower than those obtained for the cell with CGO, supporting that reactivity deteriorates the cell performance by causing an increase in the ASR values.

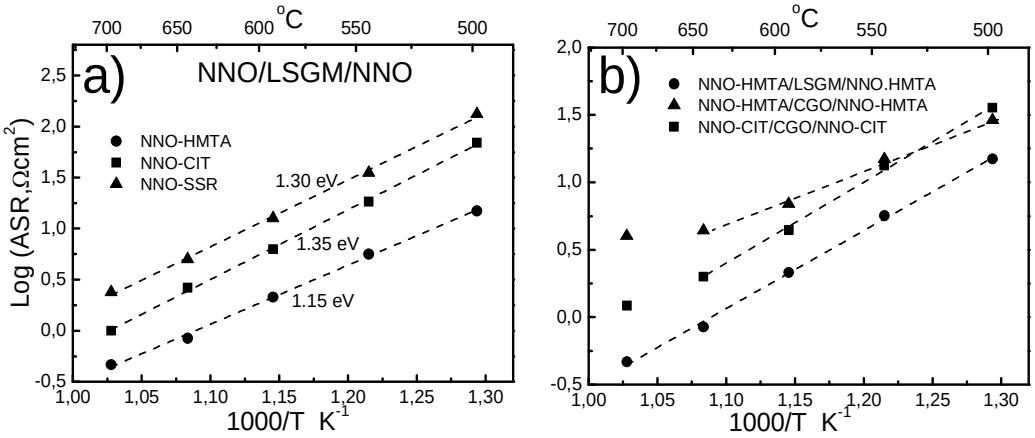

Figure 2. a) Dependence of the ASR with temperature for NNO-HMTA, NNO-CIT and NNO-SSR electrodes deposited on LSGM electrolyte. b) Comparison of ASR values for NNO-HMTA/LSGM/NNO-HMTA cell against NNO-HMTA/CGO/NNO-HMTA and NNO-HMTA/CGO/NNO-HMTA cells.

Determination of the Limiting Steps in the Electrode Reaction for NNO/LSGM/NNO Cells.

The oxygen electrode reaction involves several stages that depend essentially on temperature, pO_2 and electrode characteristics. For Mixed Ionic-Electronic Conductors, (MIEC), the presence of ionic conductivity extends the reaction zone beyond the Triple Phase Boundary (TPB). Therefore, ORR of a mixed conductor electrode takes place through several steps, consecutive (serial) or simultaneous (parallel) (23):

1. O_2 gas phase diffusion.
2. Adsorption/desorption of O_2.
3. Dissociation of molecular adsorbed oxygen.
4. Charge transfer and ionic incorporation or surface exchange into electrode surface.
5. Diffusion inside the MIEC towards the electrode/electrolyte interface (Double Phase Boundary, DPB).
6. Ion transfer through the DPB.

For each step, a relation between the polarization resistances and pO_2 values could be determined, $Rp \alpha pO_2^{-n}$, where "n" is characteristic of the process nature. The EIS spectra obtained in terms of temperature and pO_2 were fitted by equivalent circuits using the Zview program. The spectra dependence with temperature and pO_2 was analyzed and the limiting steps in the electrode reaction were identified comparing the obtained results with others reported in the literature and/or theoretical models.

Figure 3 shows, as an example, the spectrum obtained at 600 °C and pO_2 = 6.6 x10^{-4} atm for NNO-HMTA. The symbols represent the measured data and the lines are the fitted curves (elementary and overall). The equivalent circuit consists on an electrolyte resistance (Rel) in series with the inductance of electrical leads (L) and different contributions related to ORR electrode. Each electrode contribution and its pO_2 dependency are discussed below. A $RCpe_{HF}$ circuit was used to adjust the contribution of high frequency (HF), a Warburg element (W) for the contribution at Medium Frequencies (MF) and a $RCpe_{LF}$ circuits for Low Frequencies (LF). The RCpe impedance components are circuits composed by a resistance R in parallel with a Constant Phase Element (Cpe). This equivalent circuit was in agreement with those previously used to fit the EIS spectra for NNO/CGO/NNO cells (19).

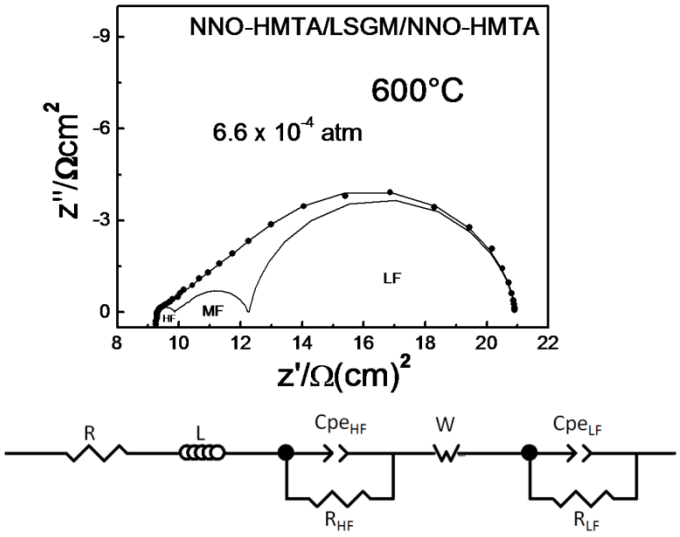

Figure 3. EIS Spectrum for NNO-HMTA at 600 °C and pO_2 = 6.6 x10^{-4} atm and the equivalent circuit used for fitting the EIS spectra.

The HF contribution was observed below 700 °C, the ASR values for this contribution did not show dependence with pO_2. This fact and the Capacitance values (C) around 10^{-6} Fcm^{-2} indicate that this step could be associated with oxygen ion transfer from the electrode to the electrolyte. The ASR of the MF contribution present a pO_2 dependence between -0.16 and -0.20 (Figure 4 a)). This dependence, of about -1/6, could be associated with interstitial O diffusion inside the cathode as limiting step. For this contribution, C values are between 3x10^{-1} and 5x10^{-1} Fcm^{-2}, in agreement with a process taking place inside the solid. These results could explain how the reactivity affects the oxygen reaction processes for MF contribution in NNO/CGO/NNO. For example, for NNO-HMTA/CGO/NNO-HMTA cell, we found that the MF depends with pO_2 as n = -1/4 because oxygen diffusion inside the solid is collimated with surface exchange (19). This could be because chemical reactivity affects the TPB and the active surface for the oxygen exchange (19). Since NNO do not react with LSGM only the oxygen diffusion is the limiting step in the MF range.

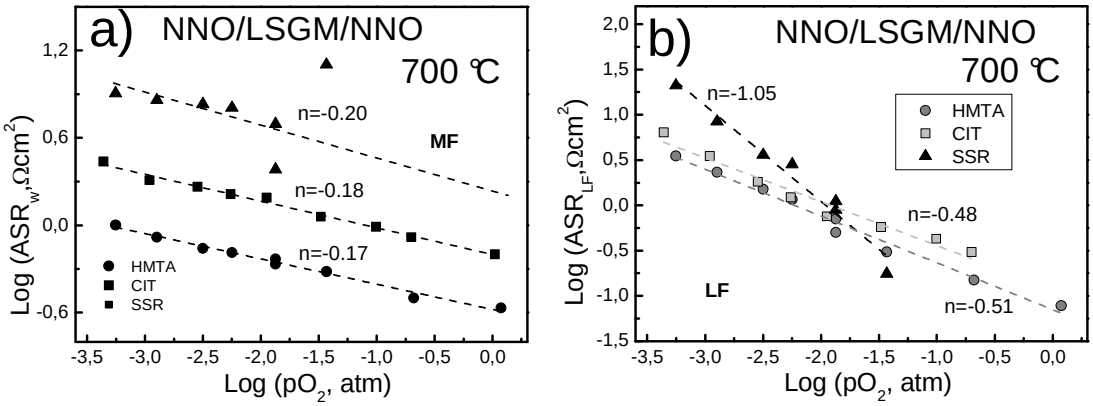

Figure 4. ASR values vs. pO_2 at 700 ºC, using a double-logarithmic representation for medium frequencies a) and low frequencies (b) contributions of NNO-HMTA, NNO-CIT and NNO-SSR electrodes.

The LF contribution was fitted by a $RCpe_{LF}$ circuit. For HMTA and NNO-CIT, n is near to -0.5 (see Figure 4 b)) and C is around 10^{-2} Fcm^{-2}. These data suggest that dissociative adsorption is the limiting step. ASR values for the NNO-HMTA sample are lower than those of NNO-CIT and NNO-SSR. These results indicate that the microstructure is the most important parameter in the electrode reaction for the surface processes.

For NNO-SSR, the LF contribution was only observed within the pO_2 range between 8 $x10^{-3}$ and 4 $x10^{-5}$ atm. The dependence of ASR with pO_2 varies as $pO_2^{-0.56}$ at 600 °C and as $pO_2^{-1.05}$ at 700 °C. C values obtained for this contribution are around 10^{-2} and 10^{-1} Fcm^{-2} at 600 and 700 °C, respectively. These C values were related to dissociative adsorption process (n = -0.5) and gas phase diffusion of O_2 (n = 1). These results suggest that the LF contribution in the NNO-SSR sample should be related to dissociative adsorption at 600 °C and to gas phase diffusion at 700 °C (Figure 4 b)). The O_2 diffusion could be a limiting step for the electrode reaction in NNO-SSR sample because of its closed microstructure and low porosity.

Conclusions

No chemical reactivity was detected between NNO and LSGM below 1050 °C by XRD. The limiting steps for oxygen reduction in NNO compound was determined through EIS. To evaluate the effect of microstructure on the electrode reaction of the NNO/LSGM/NNO cell, we compared the electrochemical response of NNO cathode by using three different synthesis routes (HMTA, CIT and SSR).

The NNO/LSGM/NNO cell with the best performance was that prepared with NNO-HMTA as electrode. The lower ASR values obtained for this cell are due to its fine microstructure composed of small particle with high active surface, which improves the oxygen reduction kinetics. In comparison with the ASR values for the NNO/CGO/NNO cells (19), the use of LSGM as electrolyte decreases the ASR values. This is due to the presence of chemical reactivity between CGO and NNO, which deteriorates the electrode performance decreasing the active surface for oxygen reduction.

Acknowledgments

This work was supported by CNEA (Argentine Atomic Energy Commission), CONICET (Argentine Research Council), UNCuyo and ANPCyT. The authors thank Mr. C. Cotaro for his technical assistance in SEM observations.

References

1. W. Feduska and A. O. Isenberg, *J. Power Sources*., **10**, 89 (1983).
2. K. Huang, *J. Electrochem. Soc*., **145**, 3220 (1998).
3. V. Dusastre and J. A. Kilner, *Solid States Ionics*., **126**, 163 (1999).
4. C. Xia, W. Rauch, F. Chen and M. Liu, *Solid State Ionics*., **149**, 11 (2002).
5. F. Mauvy, J.-M. Bassat, E. Boehm, J.-P. Manaud, P. Dordor and J.-C. Grenier, *Solid State Ionics*., **158,** 17 (2003).
6. F. Chauveau, J. Mougin, J.M. Bassat, F. Mauvy and J. C. Grenier, *J. Power Sources*., **195**, 744 (2010).
7. V. V Kharton, A. P. Viskup, A. V Kovalevsky and E. N. Naumovich, *Solid State Ionics*., **143**, 337 (2001).
8. L. Minervini, R. W. Grimes, J. A. Kilner and K. E. Sickafus, *J. Mater. Chem*., **10**, 2349 (2000).
9. S. J. Skinner and J. A. Kilner, *Solid State Ionics*., **135**, 709 (2000).
10. J. M. Bassat, P. Odier, A. Villesuzanne, C. Marin and M. Pouchard, *Solid State Ionics*. **167**, 341 (2004).
11. A. Montenegro-Hernández, L. Mogni and A. Caneiro, *Int. J Hydrogen Energy*., **35**, 6031 (2010).
12. A. Montenegro-Hernández, J. Vega-Castillo, L. Mogni and A. Caneiro, *Int. J. Hydrogen Energy*., **36**, 15704 (2011).
13. R. Sayers, J. Liu, B. Rustumji and S. J. Skinner, Fuel Cells., **8**, 338 (2008).
14. F. Mauvy, C. Lalanne, J. Bassat, J. Grenier, H. Zhao, P. Dordor, et al., *J. Eur. Ceram. Soc*., **25**, 2669 (2005).
15. H. Zhao, F. Mauvy, C. Lalanne, J. Bassat, S. Fourcade and J. Grenier, *Solid State Ionics*., **179**, 2000 (2008).
16. J. Wan, J. B. Goodenough and J. H. Zhu, *Solid State Ionics*., **178**, 281 (2007).
17. F. Chauveau, J. Mougin, F. Mauvy, J.-M. Bassat, J.-C. Grenier, *Int. J. Hydrogen Energy*., **36**, 7784 (2011).
18. L. Baque, A. Caneiro, M.S. Moreno and A. Serquis, *Electrochem. Commun*., **10**, 1905 (2008).
19. A. Montenegro-Hernández, L. Mogni and A. Caneiro, *Int. J. Hydrogen Energy*., **37**, 18290 (2012).
20. A. Caneiro, P. Bavdaz, J. Fouletier and J.P. Abriata, *Rev. Scientific Instruments*., **53**, 1072 (1982).
21. I. D. J. Scribner Associates, Zview, (n.d.).
22. Y. M. Chiang, D. P. I. Birnie and W. D. Kingery, Physical ceramics. Principles for ceramic science and engineering, 1997.
23. S. B. Adler, Chem. Rev., **104**, 4791 (2004).